Polymer Bulletin (2023) 80:12761–12786
https://doi.org/10.1007/s00289-023-04685-w

ORIGINAL PAPER

High-density amine-functionalized MCM-41 derived from pumice: facile synthesis and antibiotic adsorption

Mansur Zarrabi[1]

Received: 2 July 2022 / Revised: 24 December 2022 / Accepted: 9 January 2023 /
Published online: 13 January 2023

Abstract

The MCM-41 adsorbent was derived from Iranian natural pumice as source of silica for the first time and highly grafted with APTES for anchoring cephalexin (CEX) molecules. The parent MCM-41 had a specific surface of 913 m^2/g while the value decreased to 819 m^2/g after grafting with 6.52 µmol APTES per square meter of adsorbent surface. Batch adsorption data were best fitted onto various kinetic and isotherm model with higher correlation coefficient and lower residual sum of squares for pseudo-first-order kinetic model and Langmuir isotherm model. In this regard, amine-grafted MCM-41 (N-MCM-41) showed an excellent adsorption capacity of 56.31 mg/g according to Langmuir model. Removal efficiency was decreased by 50% in the presence of coexisting ions. Nonlinear Thomas model best fitted onto breakthrough curves at various experimental condition. For synthetic solution and at moderate condition, about 41.53 mg/g of CEX was adsorbed in continues experiment. For simulated samples, 19.74 mg/g adsorption capacity was achieved under dynamic condition. Thermal destruction method was used to recover the spent adsorbent and after six cycle adsorption–desorption, adsorption capacity decreased from 41.53 to 8.72 mg/g. Overall, the present study proposed N-MCM-41 prepared from natural pumice for effective adsorption–desorption of CEX, which could be a guidance for antibiotics adsorption.

Keywords Pumice · MCM-41 · N-MCM-41 · Column study

✉ Mansur Zarrabi
mansor62@gmail.com

[1] Department of Environmental Health Engineering, Research Center for Health, Safety and Environment (RCHSE), Alborz University of Medical Sciences, Karaj, Iran

Introduction

The exploration of the M41S materials in the early 1990s introduced new application of highly ordered mesoporous silica-based molecular sieves in the field of photonic, drug deliver, adsorption and as well as catalyst [1]. Mobil composition of matter (MCM)-41, most widely studied of this family of materials, has attracted extensive attention due to their high specific surface area, the narrow and well defined pore size distribution [2]. Besides that, the hydroxyl functional groups (Si–O–H) on the surface of MCM-41 could be modified with various functional groups through O–H bands and consequently develops its utilization [3]. In conventional method, organosilanes such as tetramethylorthosilicate (TMOS) and tetraethylorthosilicate (TEOS) are used as silica source. However, high cost and toxicity of alkoxides limit the large scale production of MCM-41 materials [4]. To address these problems, researchers used sodium silica solution derived from natural materials instead of alkoxides. Pumice is a volcanic rock mainly composed of SiO_2 (65%) that can be used as an inexpensive source of silica for manufacturing sodium silicate [5]. However, due to the presence of hydroxyl bonds and an ethereal linkage, silica-based materials have an isoelectric point below 3.5 and therefore are suitable for attracting electron-deficient species such as neutral and cationic compounds [6]. To address these issues, the hydroxyl functional groups (Si–O–H) on the surface of MCM-41 could be modified with compounds containing amine functional groups to expand isoelectric point up to 7. The 3-aminopropyl triethoxysilane (APTES), due to the its fast hydrolysis rate, containing three ethoxy groups per molecule and forming oligomers and polymers of silanes which accelerate its bonding to the silica surface, is a good candidate for surface modification of silica-based materials to present a highly powerful adsorbent for capturing both negatively and positively charged pollutants [5]. Cephalosporins antibiotics are the most assured and effective broad-spectrum bactericidal antimicrobial agents, being the most prescribed of all antibiotics [5]. Cephalexin (CEX), belong to the first-generation cephalosporin antibiotics with the same fundamental structural as penicillin, is the most widely used antibiotic for treatment of infections caused by gram-positive and gram-negative bacteria in human or animal due to its extensive bactericidal activity [7]. Cephalexin molecules contains both acidic (COOH) and basic (NH_2) functional groups on its structure and depending on solution pH, it present amphoteric properties in aqueous solution. In this regard, cephalexin would have positive charge in acidic solution ($pH < 2.56$) due to the protonation of NH_2 group, carrying negative and positive charge in pH between 2.56 and 6.88 and negative charge in $pH > 6.88$ due to the deprotonation of COOH group [8, 9]. Various methods such as adsorption [7–9], photocatalytic reduction [10, 11], electro-oxidation process [12], biological process [13], ultrasonic process [14], membrane process [15] and so on have been investigated for CEX removal. However, the cost and complexity of advanced oxidation process and membrane filtration, less efficiency, production of secondary sludge and sensitivity of activated sludge to pharmaceuticals, and the limitations of electrochemical process in field application, have resulted in

limited application of these techniques for effective removal of antibiotics [16]. On the contrast, adsorption-based processes are simple, relatively inexpensive, and not sensitive to water pollutants and considered as more established (in field application) and highly efficient processes for removal of wide range of pollutant from contaminated water sources [17]. Based on the above-mentioned facts, the present work was scheduled to prepare: (I) high purity MCM-41 from abundant and inexpensive pumice by adding ion exchange step after sodium silicate preparation, (II) grafting of MCM-41 with APTES in the presence of tetraethyl orthosilicate (TEOS) to extended high-density and strength amine group on MCM-41 surface, (III) investigate the capture of cephalexin molecules from aqueous solution in batch and dynamic mode by amine modified MCM-4 (N-MCM-41), (IV) determining the adsorption mechanism by various two- and three-parameter isotherm and kinetic models and (V) regeneration and real sample test.

Materials and methods

Chemicals

All chemical was analytical grade and used without further purification. Natural pumice samples were obtained from an open area in Tikmeh Dash, East Azerbaijan, Iran. Cetyl trimethyl ammonium bromide (CTAB), ammonia solution, hydroxybenzaldehyde (Salicylaldehyde, purity > 99%), tetraethyl orthosilicate (TEOS), ethanol (99.9%), NaOH powder and hydrochloride acid were purchased from the Merck Company (Germany). Cephalexin powder (97% purity) and Amberlite@IR120 hydrogen form resin were procured from the Sigma-Aldrich Corporation.

Synthesis of MCM-41

Sodium silicate solution was prepared as our previous work [5]. To remove the excessive cations such as sodium ions, the prepared silicate sodium solution was mixed with Amberlite@IR120 hydrogen form resin with a ratio of the resin to solution was 1:1 (v/v). The suspension was mixed until the pH was reached to 8.5. The obtained solution was used as silica source. To prepare MCM-41, 2.3 g of cetyltrimethylammonium bromide was added to 53 mL of as prepared sodium silicate solution and mixed slightly to get a homogenous solution. As suspension was stirred, 21 mL of ammonia solution was added drop wise to the suspension until a white gel was obtained. The obtained white gel was stirred for 3 h and then aged in a mixture of ethanol/water (1:1 ration) for 24 h at room temperature. After aging, the white was washed with distillated water until the recorded pH reached to 7.5. The unused CTAB was removed by heating the white get at 550 °C for 6 h. Finally, the calcined MCM-41was used in future experiments.

Modification of MCM-41

MCM-41 was functionalized with 3-aminopropyl triethoxysilane (APTES) to extend the positive charge on its surface. To do that, 2.5 g of as prepared MCM-41 was added to 100 mL dried ethanol and stirred to obtain a homogenous suspension. About 2 mL of TEOS was added to suspension and stirred for 2 min. During stirring, 2.5 mL of APTES solution was added dropwise and mixed for next 10 min. The suspension was then refluxed at 70 °C for 30 min and then cooled to room temperature. Finally, the suspension was filtered, washed with deionized water and dried at 80 °C for 24 h. the final product was labeled as N-MCM-41 and used in adsorption experiment [5]. Schematic of MCM-41 synthesis and modification is depicted in Fig. S1.

Material characterization

The MCM-41 and N-MCM-41 were characterized by several techniques to determine their textural properties, surface morphology and functional groups. The crystalline phase of MCM-41 and N-MCM-41 was determined by an X-ray diffractometer (XRD, PHILIPS-model PW-1730, Netherlands), using CuKα radiation (wave length of 1.54056 Å with a step width of 0.02°, and a scan rate of 1°/s) operated at 40 kV and 30 mA. The surface morphology of MCM-41 and N-MCM-41 samples were investigated by field emission scanning electron microscopy using a FESEM-ESCAN device (model Mira III, Czech Republic) equipped with energy dispersive X-ray spectroscopy (EDX). Fourier transform infrared spectroscopy (Perkin Elmer-spectrum 65, USA) was used to identify the functional group type of the prepared adsorbents at wave number range 400–4000 cm^{-1} using KBr disks (samples to KBr ratio of 1:7). The adsorption–desorption test was conducted at 77 K (Belsorp mini, Japan). Before analysis, the sample was degassed at 150 °C for 4 h, under vacuum. The point of zero charge of the MCM-41 and N-MCM-41 was determined by adding 0.1 g of adsorbents into 6 Erlenmeyer flasks filled with 50 mL of 0.1 M NaCl solution, where the initial pH was adjusted to 2–12 using 1 M NaOH or 1 M HCl solutions. Then, the flasks were agitated at 300 rpm for 2 days, and the final pH results were recorded. The pH_{pzc} of the adsorbent represents the intersection point between the final and initial pH curves [5].

Amine leachate test

The stability of the amine groups on the surface of N-MCM-41 was tested by the Schiff base reaction [18]. For do this, 2.5 g of N-MCM-41 was added to 100 mL ethanol in a polypropylene flask, mixed for 2, 4, 6, 8 and 10 h at 350 rpm using a shaker (Hanna-Hi 190 M, Singapore). After time elapsed, the samples were filtered to remove the solid phase and supernatant was used to investigate the leached amine. To do that, about 0.5 mL salicylaldehyde was added to a 5 mL of filtrate; resulting in a bright yellow color that could be analyzed at 404 nm using a spectrophotometer (Shimadzo-1700, Japan).

Batch adsorption experiment

The stock CEX solution was prepared by dissolving the appropriate amount of powdered CEX in solution containing 950 mL deionized water and 50 mL 1 M NH_4OH and kept in glass container at room temperature. Batch adsorption experiments were conducted in 250 mL polyethylene flasks by varying one parameters and keeping other parameters constant. Experimental parameters were solution pH (4–8), N-MCM-41, reaction time (10–150 min) and initial CEX concentration (5–25 mg/L). In all experiments 0.2 g/L N-MCM-41 was used. The initial pH of the working solutions was adjusted by addition of 0.1 M NaOH and/or H_2SO_4. After each experiments, the absorbance of remained CEX was measured using UV/VIS spectrophotometer (model 1700, Shimadzu, Japan) at the wave length peak of 261 nm. After optimizing the experimental parameters, the time-solute concentration was utilized for kinetic modeling. To determine isotherm parameters, various CEX concentration ranging from 2 to 20 mg/L at optimal pH was shacked with 0.2 g/L of N-MCM-41 until equilibrium time reached. The obtained data were then analyzed by various two- and three-parameter isotherm models. To test the ability of N-MCM-41in real condition, a solution containing of various ions such as phosphate (1 mg/L), hardness (80 mg/L), sulfate (30 mg/L), fluoride (0.5 mg/L), chloride (30 mg/L) aluminum (0.1 mg/L), copper (0.1) and nitrate (10 mg/L) was prepared. After adding appropriate amount of CEX and 0.2 g/L N-MCM-41 to each solution, the solution was shacked until equilibrium time reached.

Column adsorption experiment

A Plexiglass column with 15 cm length and 1 cm inner diameter was used to study the dynamic adsorption of CEX onto N-MCM-41 (Fig. S2). The adsorbent was grinded and sieved to 104 μm (mesh 140) and packed to column according to studied length. Different concentration of CEX solution (2, 10 and 20 mg/L) was prepared and passed through the column at different flow rate (5, 10 and 15 mL/min) and column length (5, 10 and 15 cm) using peristaltic pump (Longer basic model) to determine the breakthrough point of column. In the present work, the breakthrough point refers to a point in which the effluent concentration reaches to about 5% of influent concentration. CEX solution of known concentration was continuously pumped into the column upward at room temperature. The samples from outlets at different height were analyzed for the final concentration. The schematic of present setup is shown in Fig.S2. Similar to batch adsorption experiment, simulated CEX solution was prepared by adding appropriate amount of coexisting ions to CEX solution and passed through the column at optimal condition.

Regeneration of N-MCM-41

Thermal method was used to investigate the reusability of exhausted N-MCM-41. To do this, the exhausted N-MCM-41 from column experiment was collected and

refluxed at 80 °C in deionized water for 2 h. Finally, the recovered adsorbent was dried at 105 °C for 24 h and used in column mode to investigate the regeneration efficiency. The regeneration-reusability cycles were repeated until the adsorbent loosed 30% of initial capacity.

Results and discussion

Material characterization

Natural pumice sample is composed mainly SiO_2 (i.e., 63.45%) and Al_2O_3 (i.e., 17.24%), resembling natural zeolite composition and good candidate as silica sources in preparing silicates compound. The XRD, XRF, SEM and FTIR properties of natural pumice has been presented in our previously published work [5, 19]. Figure 1 shows the small angle XRD patterns of the MCM41 and N-MCM-41. Three dominant peaks at $2\theta = 1.90°$, 3.60° and 4.30° corresponded to (100), (110) and (200) diffractions could be observed (100) is attributed to the hexagonal structure of prepared MCM-41 [4]. For N-MCM-41, the intensity of peak (100) still remained; demonstrating the higher hexagonal mesoporous structure of sample after APTES grafting. However, the lower intensity of (100) and inappreciative peaks of the higher odder (110) and (200) diffractions implied a poorly ordered structure of the functionalized adsorbent and evidence of successfully APTES grafting on the mesoporous channel surface [1].

The nitrogen adsorption–desorption isotherm and pore size distribution of MCM-41 and N-MCM-1 samples are depicted in Fig. 2. Both adsorbent exhibited a Type IV isotherm model with H3 hysteresis loops and steep increase in the nitrogen uptake at P/P_o ~0.40 associated with characteristic feature of highly mesoporous substances according to the IUPAC classification [20]. The parent sample (Fig. 2a) had a specific surface of 913 m^2/g, pore volume of 0.97 cm^3/g, and the average

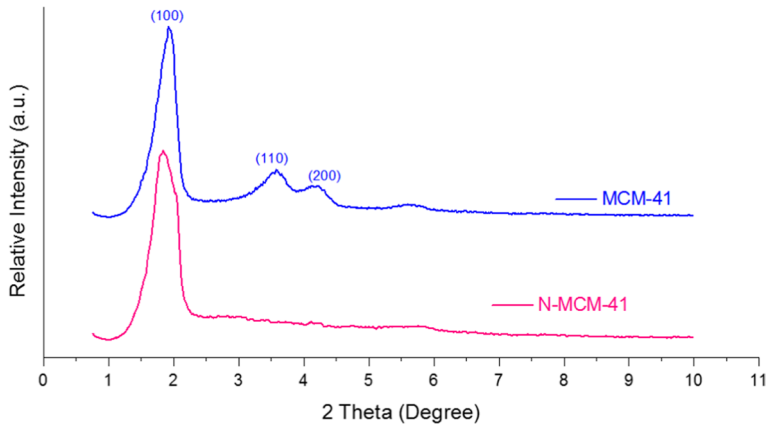

Fig. 1 XRD patterns for the MCM41 and N-MCM-41

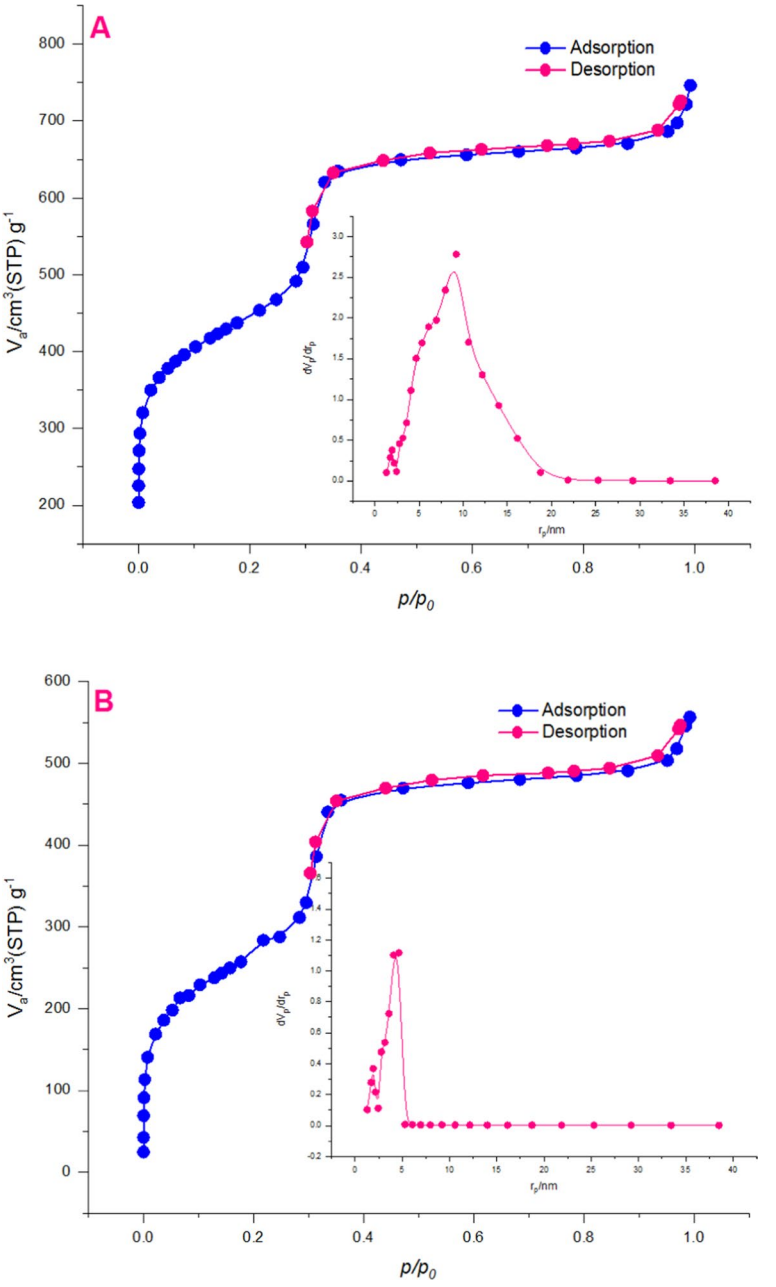

Fig. 2 Nitrogen adsorptions–desorption isotherm and pore size distribution of MCM-41 (**a**) and N-MCM-41 samples (**b**)

diameter of pore of 8.78 nm. When the APTES was grafted on mesoporous channel surface of MCM-41, specific surface, pore volume and average diameter of N-MCM-41 were decreased to 819 m^2/g, 0.62 cm^3/g, 6.43 nm, respectively. This phenomenon is due to the occupancy of structural channels by amino groups [6].

The FTIR spectra of the MCM-41 and N-MCM-41 samples are depicted in Fig. 3. In both sample, a broad band observed at 3410 cm^{-1} can be assigned to the H-bonded silanol groups (Si–OH) corresponding to the physisorbed water molecules [21]. Typical characteristic peaks of silica observed at 459, 795 and 1080 cm^{-1} which can be assigned to the vibrations of the Si–O–Si symmetric bond, Si–OH stretching bond and Si–O–Si asymmetric bond, respectively [22]. In N-MCM-41 sample, a narrow and weak peak was observed at 2937 cm^{-1} that can be assigned with CH_2 groups present in the hydrocarbon chain of amino silane compounds [2]. In addition, the peak at 678 and 1640 cm^{-1} can be attribute to the bending vibration of C-N and symmetric bending vibration of NH2 groups of in the N-MCM-41 surface [23].

The microstructure, surface morphology and EDX results of MCM-41 and N-MCM-41 samples are illustrated in Fig. 4. FESEM image of parent MCM-41 (Fig. 4a) revealed a regular surface and uniform distinct spherical pieces with particle diameter in the range of 20–100 nm. After APTES grafting (Fig. 4b), the particles show some agglomeration and accumulation due to the formation of a bridge between the mesoporous MCM-41 structure and APTES molecules [24]. According to EDX results (Fig. 4c) main components of MCM were silicon (41.52%w) and oxygen (58.48%w), which demonstrating the successful ion exchange occurring in the initial sodium silicate. The main components of N-MCM-41 (Fig. 4d) were silicon (25.14%w), oxygen (49.18), nitrogen (17.14%w) and carbon (8.54%w) according to the EDX results. The increase in components of N-MCM-41 demonstrate the incorporation of APTES in MCM-41 structure. In addition, elemental mappings of N-MCM-41(Fig. 4e) confirmed the presence of nitrogen in sample structure.

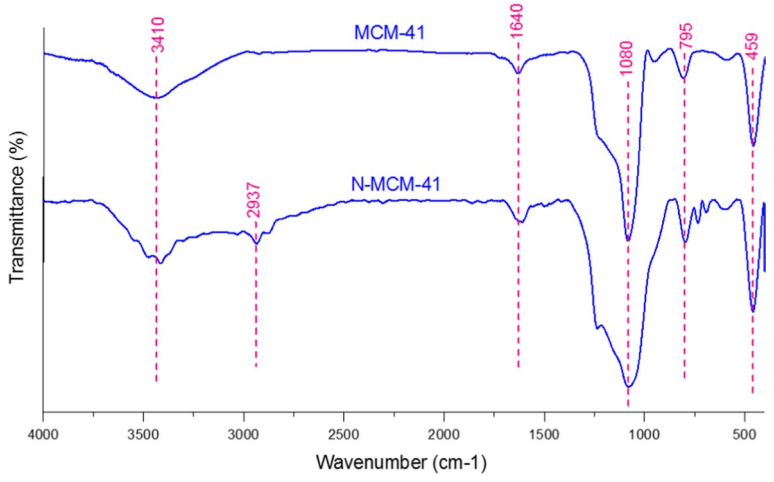

Fig. 3 FTIR spectra of MCM-41 and N-MCM-41

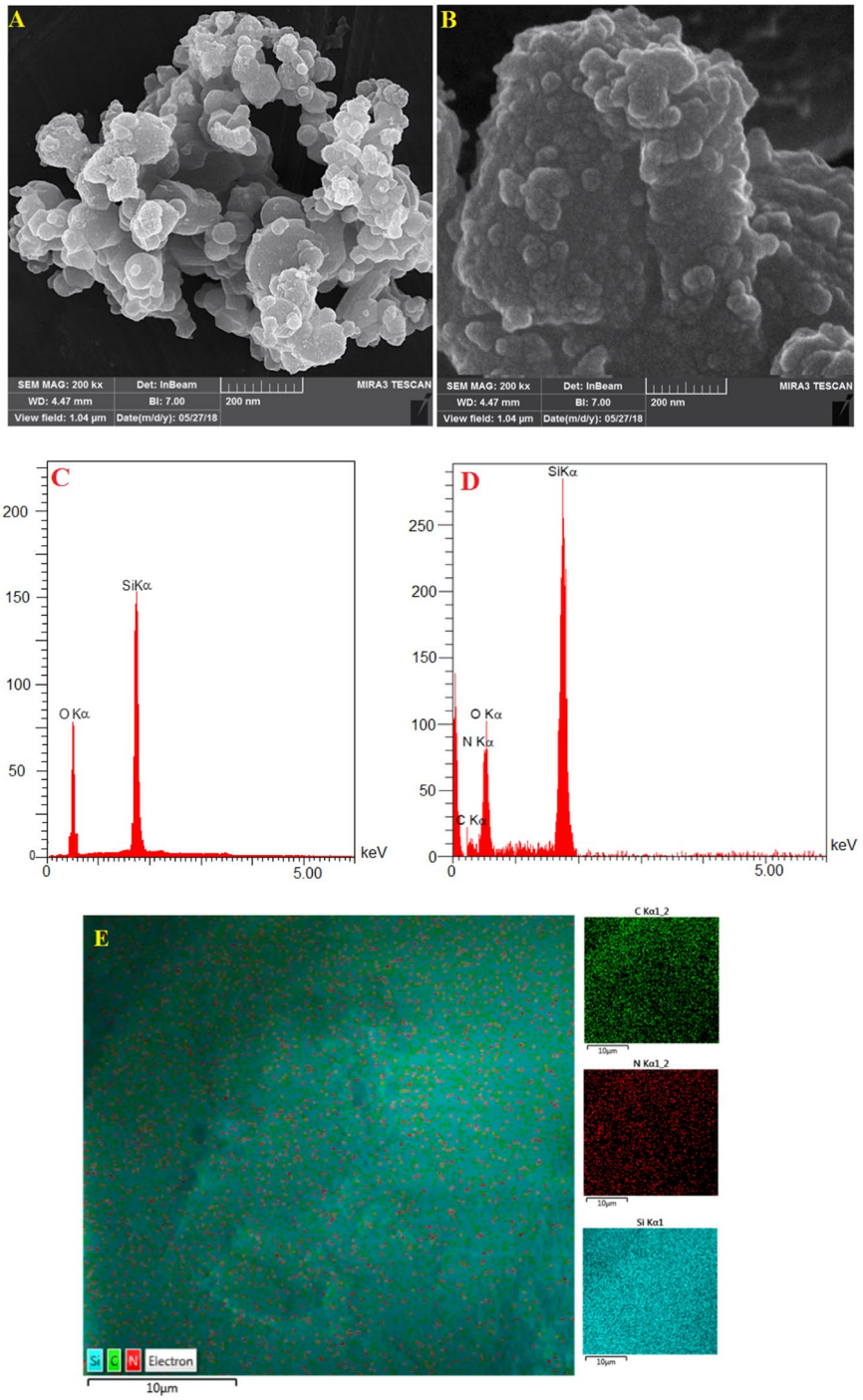

Fig. 4 FESEM of MCM-41 (**a**) and N-MCM-41 (**b**); EDX of MCM-41 (**c**) and N-MCM-41 (**d**) and Elemental mappings of N-MCM-41 (**e**)

According to Fig.S3, surface of parent MCM-41 was negatively charged at pH > 3.20 due to the presence of Si–OH groups. Therefore, parent MCM-41 surface is not suitable for capturing negatively charged molecules at pH > 3.20. By grafting of amine group on parent MCM-41, the zero-point charge of sample increased to 8.30; implies that N-MCM-41 will be positively charged at pH below 8.30 and negatively charge at pH above 8.30. This phenomenon is mainly due to the replacement of the silanol groups with amine groups, which tends to gain protons and renders a net positive charge on the modified sample surface [25].

Figure 5 represents the thermo-gravimetric analysis (TGA) of prepared samples. MCM-41 sample showed a 1% weight loss below 100 °C which can be attributed to molecules of adsorbed water being release from the surface of the sample. From 100 to 900 °C, no change is observed in sample weight which demonstrate the high thermal stability of MCM-41 [21]. For N-MCM-41 two distinct mass losses was observed. First, negligible mass losses observed below 200 °C, caused by molecules of physisorbed amino silane moieties. The second one was a sharp weight loss from 250 to 700 °C and reached a plateau around after 700 °C. Such sharp weight loss is mainly due to the decomposition of the APTES molecules incorporated to the N-MCM-41 sample [26].

Aminosilanes can significantly enhance the adsorption of biomolecules on silicates surfaces via introducing positive charge or electron-rich nitrogen atoms into the structure [27]. However, the physicochemical stability of the grafted aminosilanes on aerogel surface is not studied clearly. Three different types of bonds are involved in grafting of aminosilanes on silica-based surfaces [28] including: (a)

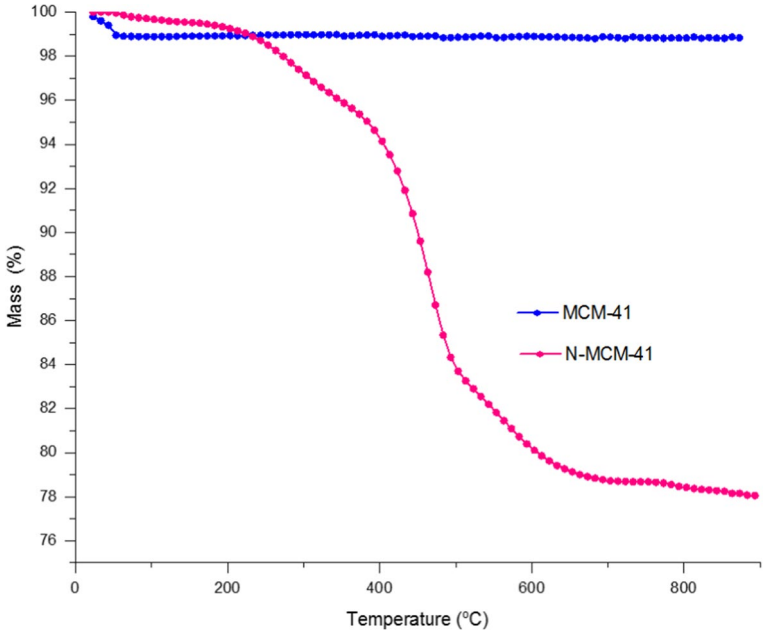

Fig. 5 The TGA curves of MCM-41 and N-MCM-41

hydrogen bonding of aminosilanes with surface hydroxyl groups on silica surfaces, (b) ionic bonding which may occur when a proton from silanol group is reacted with the basic amine function of the modifier, and (c) covalent interaction where the silanes react with silanol groups on silica surface. It is well known that the covalent and ionic bonded amines are more stable than the hydrogen bonded amines. It has been shown that the hydrogen bonded amines can be desorbed from silica surface by ethanol solution [18]. Figure 6 shows the UV/VIS spectra of pure 2.50% APTES solution and the filtrate of N-MCM-41 sample after reacting with 0.5 mL salicylaldehyde. As indicated in Fig. 6a, the value of absorbance of 2.50% APTES solution at 404 nm was 3.84 in comparison to 0.098, 0.153, 0.245, 0.431 and 0.439 (Fig. 6b) for the filtrate of the N-MCM-41 samples after 2, 4, 6, 8 and 10 h reacting with ethanol, respectively. In complete monolayer grafting, each APTES molecule occupies about 50 square angstrom corresponded to 3.32 µmol/m^2. On the other hands, 2.50% APTES solution is corresponds to 6.52 µmol APTES per square meter of adsorbent surface. According to Fig. 7b, more than 0.025%, 0.039%, 0.064%, 0.112% and 0.114% of grafted APTES was leached during 2, 4, 6, 8 and 10 h reacting with ethanol, respectively. This mean that more than 89% of APTES was grafted onto N-MCM-41 which is corresponds to 6.13 µmol APTES per square meter of sample surface [18]. Based on the Schiff base reaction, lower absorbance is correlated with lower amount of amine in solution as well as with the higher stability of tested samples in water/aqueous solution. Such higher grafting rate resemble the multilayer APTES coverage on N-MCM-41 surfaces [29]. Therefore, the Schiff base reaction results confirmed higher stability of multilayer grafted APTES on N-MCM-41 surfaces. Grafting condition has important role in bonding of APTES molecules on silicates surface. First, ethanol would prevent fast hydrolysis and condensation of APTES, decreasing agglomeration of APTES oligomers, and eventually increases

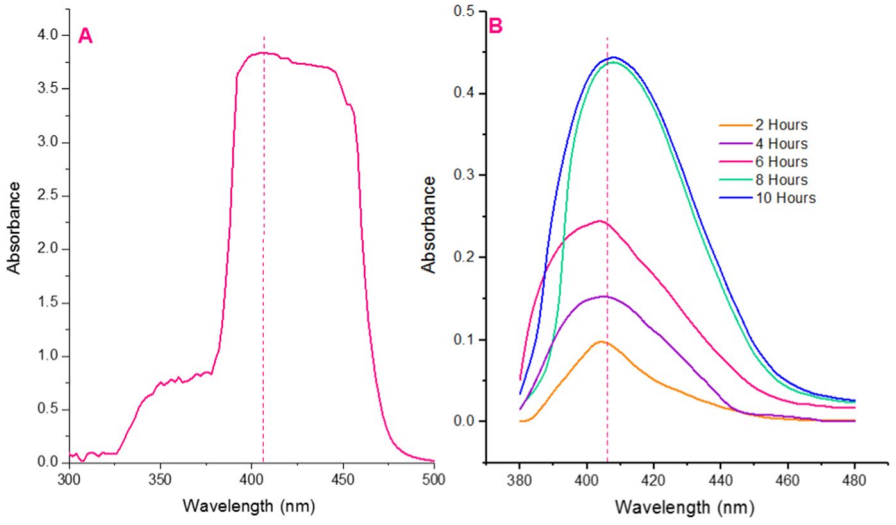

Fig. 6 V/VIS spectra of 2.5% pure APTES solution (**a**) and UV/VIS spectra of N-MCM-41 filtrate after reacting in ethanol (**b**)

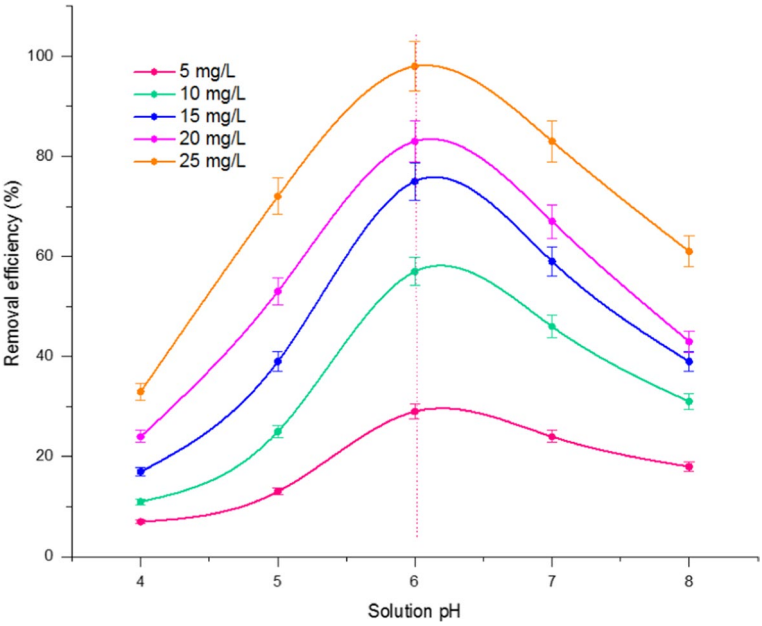

Fig. 7 Effect of solution pH and CEX concentration on removal efficiency (adsorbent 0.2 g/L and 90 min contact time)

the reactivity of APTES to join on the N-MCM-41 surface [30]. Second, chemical interaction between the chains of Si–O–Si and APTES and also between two neighboring APTES (horizontal polymerization) will accelerate at higher temperature [31]. In addition, at higher temperature the hydrolysis of APTES would increase and lead to more available ethoxy groups to react with the hydroxyl groups on the N-MCM-41 surface. Finally, the presence of a co-hydrolyzer such as TEOS will enable a fast and stable grafting process [22]. By such grafting condition, high density of the amine was grafted on the MCM-41 if compared with previously studied methods [32–34]. Taken together, these findings demonstrate that the APTES can be successfully loaded on pumice derived MCM-41 with a negligible leaching and high stability by grafting methods used in this study.

Effect of solution pH and CEX concentration

Solution pH and solute concentration have significant role in adsorption of CEX on N-MCM-41 surface. Solution pH can influence the surface charge of the adsorbent and solute molecules. As indicated in Fig.S3, the pH_{zpc} of N-MCM-41was 8.30, thus the net surface charge of the adsorbent remains positive at $pH < 8.30$ and negative at $pH > 8.30$. On the other hands, the pH of solution will affect the degree of ionization and speciation of solute. Cephalexin is a zwitterionic molecule with pK_a values of 2.56 (carboxylic acid group) and 6.88 (weakly basic aminothiazole group). Therefore, CEX is anionic charged at pH 6.88 and above, at pH values below 2.56 it

is cationic, existing as a zwitterion species between both pK_a values [35]. Figure 7 shows the effect of solution pH and initial CEX concertation on removal efficiency. As indicated, removal efficiency was increased with increase in solute concentration. This fact can be explained by considering the higher driving at higher solute concentration. Higher solute concentration increases the driving force from the solution toward the adsorbent to overcome the mass transfer resistance at higher solute concentrations, which resulted in higher removal efficiency [9]. In addition, CEX was removed at all studied pH with higher removal at pH 6 and hampered adsorption process beyond and below pH about 6. This phenomenon can be explained by different species of solute at different pH values. At 2.56, both adsorbent and CEX surface is occupied with positive charge, thus CEX may adsorbed via π-π interaction. As pH increased from 3 to 6, adsorbent surface is still positively charged while CEX is in its zwitterion form. Therefore, electrostatic interaction will be the predominant adsorption mechanism. At pH 6 and above repulsion between negatively charged adsorbent surface and anionic form of CEX will decrease the adsorption rate [36]. Our result is in good agreement with previously published work. Accordingly, in adsorption of CEX by walnut shell-based activated carbon and Octenyl Succinic Anhydride starch [7, 37] higher removal efficiency has been reported at pH 6 and higher solute concentration. However, higher removal efficiency of CEX by zirconium-based metal–organic frame work due to the coordination interactions between the inorganic clusters of MOFs and the organic groups of cephalexin at higher pH value has been reported [38].

Kinetic of CEX adsorption

In the present work, the nonlinear form of pseudo-first-order, pseudo-second-order and intra-particle diffusion model have been used to describe the adsorption of CEX

Table 1 Parameters of kinetic models used for Cephalexin adsorption by N-MCM-41

Kinetic model	Parameters	10 mg/L	20 mg/L
Pseudo-first order: $\frac{dq_t}{dt} = k_1(q_e - q_t)$	k_1(1/min)	0.014	0.014
	$q_{e\cdot Exp}$	9.60	19.17
	$q_{e\cdot Cal}$	11.43	23.42
	R^2	0.97	0.96
	RSS	3.26	21.45
Pseudo-second order: $\frac{dq_t}{dt} = k_2(q_e - q_t)^2$	k_2(g/mg min)	0.006	0.003
	$q_{e\cdot Exp}$	9.60	19.17
	$q_{e\cdot Cal}$	16.84	34.94
	R^2	0.96	0.95
	RSS	4.34	27.22
Intra-particle diffusion: $q_t = k_i t^{0.5}$	k_i(mg/g/min$^{0.5}$)	1.02	2.17
	R^2	0.94	0.92
	RSS	6.72	39.13

on N-MCM-41 adsorbent. Fig.S4 shows the fitting of time-concentration profile onto used kinetics models and related parameters are collected in Table 1. As evidence from Table 1, the kinetic data at two different concentrations were best fitted onto all studied models with higher correlation coefficient (R^2) and lower residual sum of squares (RSS) onto pseudo-first order. The closeness of $q_{e\cdot Exp}$ to $q_{e\cdot Cal}$ from pseudo-first-order model demonstrating the ability of the model in more accurate prediction of equilibrium adsorption capacities. The pseudo-first-order kinetic model assumes that one solute molecule is adsorbed onto one sorption site on the adsorbent surface and then, describes sorption in solid–liquid systems based on the sorption capacity of solids [39]. On the other hands, for process obey pseudo-first-order model, the variation in adsorption rate should be proportional to the first power of solute concentration [40]. However, if the relationship between the solute concentration and the adsorption rate is not linear, pore diffusion can limit the adsorption process. For present work, the variation in adsorption rate was proportional to the initial CEX concentration; therefore, the pore diffusion is not the limiting step. Based on this finding, the used CEX concentration was not high enough. According to pseudo-second-order model, adsorption rate decreased to half when solute concentration exceed twice. Intra-particle diffusion model is another kinetic model which is usually used to determine the rate-limiting. Based on this model, film diffusion is negligible and intra-particle diffusion is the only rate controlling step. Therefore, the amount of adsorbed solute is proportional to the square root of contact time and the straight line of $\log q_t$ vs.$0.5\log t$ should pass through the origin with a positive intercept. The plot of intra-particle diffusion model did not pass through the origin and hence intra-particle diffusion was not the rate-determining step; as demonstrated by the pseudo-first-order model. Based on our finding, bulk movement of solute to the external surface of the adsorbent and formation of solutes bond around active sorption site may limits CEX adsorption onto N-MCM-41.

Equilibrium modeling

Several two and three-parameter models were used to describe the relationship between the amount of adsorbed CEX on the adsorbent and the concentration of dissolved CEX in the liquid at equilibrium state. Theoretical aspect of used equilibrium equation has been reported in our previous work in details [5]. Fig.S5 shows the nonlinear fitting of equilibrium data on two- and three-parameter isotherm models and the related data are collected in Tables 2 and 3. As illustrated in Fig. S4 and evidence from Tables 2 and 3, equilibrium data were best fitted onto all used model with higher correlation coefficient and lower RSS (residual sum of squares) for Langmuir isotherm model. Langmuir isotherm model assume that all adsorption sites have equal energy for solute molecules and the adsorption at one site does not affect the adsorption of molecules at an adjacent site. As a result, in a monolayer adsorption, the maximum adsorption capacity is determined by the number of adsorption sites. The maximum adsorption capacity of N-MCM-41 adsorbent was 56.31 mg/g. Based on this model and pseudo-first order, monolayer adsorption of CEX onto N-MCM-41 approved. According to Freundlich model, the value of

Table 2 Two-parameter isotherm models used for Cephalexin antibiotic adsorption by N-MCM-41

Freundlich $q_e = K_f C_e^{1/n}$	K_f	n	R^2	RSS
	6.72	1.50	0.98	15.68
Langmuir $q_e = \frac{q_m b C_e}{1+bC_e}$	q_m	B	R^2	RSS
	56.31	0.13	0.99	7.38
Temkin $q_e = \left(\frac{RT}{b_1}\right) \times \ln\left(k_t C_e\right)$	B_T	A_T	R^2	RSS
	9.11	2.06	0.93	53.20
Elovich $\frac{q_e}{q_m} = K_E C_e e^{-\frac{q_e}{q_m}}$	K_E	q_m	R^2	RSS
	0.011	14.63	0.98	9.56
Dubinin–Radushkevich $q_e = \left(q_s\right) e^{\left(-K_{ad}\varepsilon^2\right)}$	q_s	K_{ad}	R^2	RSS
	28.81	7.09	0.91	72.35
Jovanovich $q_e = q_{max}\left(1 - e^{\left(-k_J C_e\right)}\right)$	q_{max}	k_J	R^2	RSS
	14.63	0.01	0.99	9.68

Table 3 Three-parameter isotherm models used for Cephalexin antibiotic adsorption by N-MCM-41

Khan $q_e = \frac{q_m b_k C_e}{\left(1+b_k C_e\right)^{a_k}}$	q_m	b_k	a_k	R^2	RSS
	64.73	0.18	10.62	0.99	8.15
Toth $q_e = \frac{q_{mT} C_e}{\left(a_T + C_e\right)^{\frac{1}{t}}}$	k_T	a_T	t	R^2	RSS
	40.87	21.03	1.50	0.98	8.96
Hill $q_e = \frac{q_H C_e^{n_H}}{K_D + C_e^{n_H}}$	q_H	n_H	K_D	R^2	RSS
	56.29	1.17	8.82	0.99	8.38
Sips $q_e = \frac{q_{ms} k_s C_e^{ms}}{1+k_s C_e^{ms}}$	q_{ms}	k_s	ms	R^2	RSS
	53.17	0.12	1.03	0.98	9.34
Redlich–Peterson $q_e = \frac{K_R C_e}{1+a_R C_e^g}$	K_R	a_R	g	R^2	RSS
	6.37	0.11	0.89	0.99	9.38

constant n was 1.5, indicating the favorable adsorption mechanism and heterogeneity of the adsorbent surface. In addition, higher value of tendency factor ($K_f = 6.72$) is a sign of high affinity of CEX molecules toward N-MCM-41 surface. From Temkin model, a high value of b_1 and k_t imply a fast sorption of solute at initial stage and strength bonding of solute onto the N-MCM-41 surface. Based on this model the higher values of b_1 and k_t demonstrating the highest adsorption of cefixime at initial stage and strength bonding with adsorbent surface. The Elovich equation is derived from adsorption kinetic and assume that the adsorption sites increase exponentially with adsorption and which is an indicative of the multilayer adsorption. Nevertheless the higher correlation coefficients and lower RSS, the value of q_m from Elovich equation was than lower those calculated from Langmuir. This indicate that a multilayer adsorption was not occurred in the studied concentration range. However, the heterogeneity of the N-MCM-41 surface can be deduced from this model. The Dubinin–Radushkevich isotherm is similar to Langmuir isotherm model and

has not the limitation of Langmuir equation such as equipotential of sorption sites, absence of steric hindrances between adsorbed and incoming particles, and surface homogeneity on microscopic level. The value of q_s from Dubinin–Radushkevich isotherm was 28.81 mg/g, which was about half of the Langmuir constant (q_m). The values of mean free energy (E) from Dubinin–Radushkevich isotherm was 0.27 (kJ/mol) which is an indication of physico-sorption nature of CEX by N-MCM-41 adsorbent. Nevertheless, Dubinin–Radushkevich model best describe the equilibrium data when intermediate ranges of solute concentrations are used. In the present work, lower correlation coefficient and higher RSS values Dubinin–Radushkevich isotherm may be due to the investigated CEX concentration. Jovanovich isotherm model is a derivation of the Langmuir model with considering some mechanical contacts between solute and adsorbent surfaces. The value of maximum sorption capacity obtained from the Jovanovich equation was 14.63 mg/g, which was half of value obtained from Dubinin–Radushkevich model (q_s) quarter of the Langmuir constant (q_m). Among three parameters isotherm model, equilibrium data were best fitted onto Khan equation. This model is a combination of Langmuir and Freundlich type. It is useful for describing both multicomponent and single component adsorption systems. According to Khan equation, adsorption of CEX onto N-MCM-41 is a combination of monolayer and multilayer phenomena. However, the maximum adsorption capacity calculated from Khan model was close to obtained value from Langmuir model, the correlation coefficient and RSS was higher than Langmuir model. The Toth isotherm model is developed empirically to improve Langmuir isotherm and reduce the error between experimental data and predicted value in porous adsorbents. This model is useful for describing heterogeneous adsorption systems and accurately best fit both low- and high-end boundary of solute concentration. The Toth model is reduced to the Langmuir isotherm equation when parameter t is equal to unity. The more the parameter t deviates from unity, the more heterogeneous is the system. The maximum adsorption capacity from Toth model was 40.87 mg/g. Parameter t was higher than unity which is as indication of heterogeneity of the adsorbent surface. The Hill isotherm model was developed to describe the binding of different species onto homogeneous substrates. This model assumes that adsorption is a cooperative phenomenon and the bonding of one solute at one site influencing the other bonding sites on the same adsorbent. The value of maximum adsorption capacity from Hill model was 56.29 mg/g which was very close to Langmuir and Khan values. The n_H was higher than unity; demonstrating the presence of positive cooperativity of one CEX molecules on other CEX molecules. The Sips isotherm model has been developed to recognize the problem of the continuing increase in the adsorbed amount with an increase in concentration of the sorbate in the Freundlich equation. Similar to the Freundlich equation, Sips model predicts a monolayer sorption capacity for high sorbate concentrations and reduces to Freundlich equation for lower sorbate concentrations. According to the Sips isotherm model, the maximum sorption capacity was 53.17 mg/g, which was very close to obtained values from Langmuir, Khan and Hill isotherm models. According to this model, monolayer sorption approved as demonstrated from other investigated models. The Redlich–Peterson (R–P) isotherm is developed by combining the Langmuir and Freundlich isotherms to amends the inaccuracies. This model assume that

the adsorption mechanism is unique and does not follow ideal monolayer adsorption. The ration of K_R to a_R which indicate the maximum adsorption capacity was 57.90 mg/g; in accordance to values obtained Sips, Langmuir, Khan and Hill isotherm models. The values of g was close to unity which reduce the Redlich–Peterson (R–P) isotherm to Langmuir model at studied concentration range. Overall, the results of equilibrium study well demonstrated the monolayer adsorption of CEX onto N-MCM-41 heterogeneous surface with about 55 mg/g maximum adsorption capacity. Table 4 presents the maximum adsorption capacity of various used adsorption in removal of CEX. As clear from Table 4, the present N-MCM-41 adsorbent showed good results if compared with previously investigated ones.

Effect of coexisting ions

To overcome the limitation of real sample, effect of various coexisting ions was investigated. In addition, to investigate the possible co-precipitation, complex formation and adsorption between CEX molecules and adsorbent, a solution containing CEX and coexisting ions was prepared and shacked in the absence of adsorbent until equilibrium time reached. The results are shown in Fig. 8. As clear from Fig. 8a, no co-precipitation, complex formation and adsorption between CEX molecules and adsorbent was occurred as the UV/VIS spectra of CEX did not changed in the presence of co-ions. Figure 8b shows the removal efficiency of CEX in the presence of co-ions and 0.2 g/L of adsorbent at pH about 6.50. In the absence of coexisting ions, the removal efficiency was 98% ("Effect of solution pH and CEX concentration" section), while, in the presence of foreign anions the removal efficiency decreased to 93%, 88%, 83%, 81%, 79%, 65%, 57% and 51% for hardness, fluoride, sulfate, nitrate, chloride, phosphate, aluminum and copper ions, respectively. Various phenomena such as changes in ionic strength, changes in solution pH and competing of foreign ions with CEX to adsorb on adsorbent may be involved in the reduction of removal efficiency. Salts are strong electrolytes that completely dissociate into ions in water and then will affects the pH and ionic strength of a solution. However, the used salt concentration was not so high to change the ionic strength remarkably, but removal efficiency was decreased. This

Table 4 maximum adsorption capacity of various adsorbent in removal of CEX

Adsorbents	Adsorption capacity (mg/g)	Reusability	Refs
Activated carbon	17.40	–	[41]
Bentonite	10.40	–	[41]
Natural zeolite	16.1	–	[35]
Fe_3O_4 coated zeolite	24.9	–	[35]
MnO_2 coated zeolite	24.5	–	[9]
Alligator weed-activated carbon	45	–	[42]
Aloe vera leaf waste (Av-S-Ac)	25.56	–	[43]
Aloe vera leaf waste (Av-N-Ac)	26.34	–	[44]
N-MCM-41	55	6	Present work

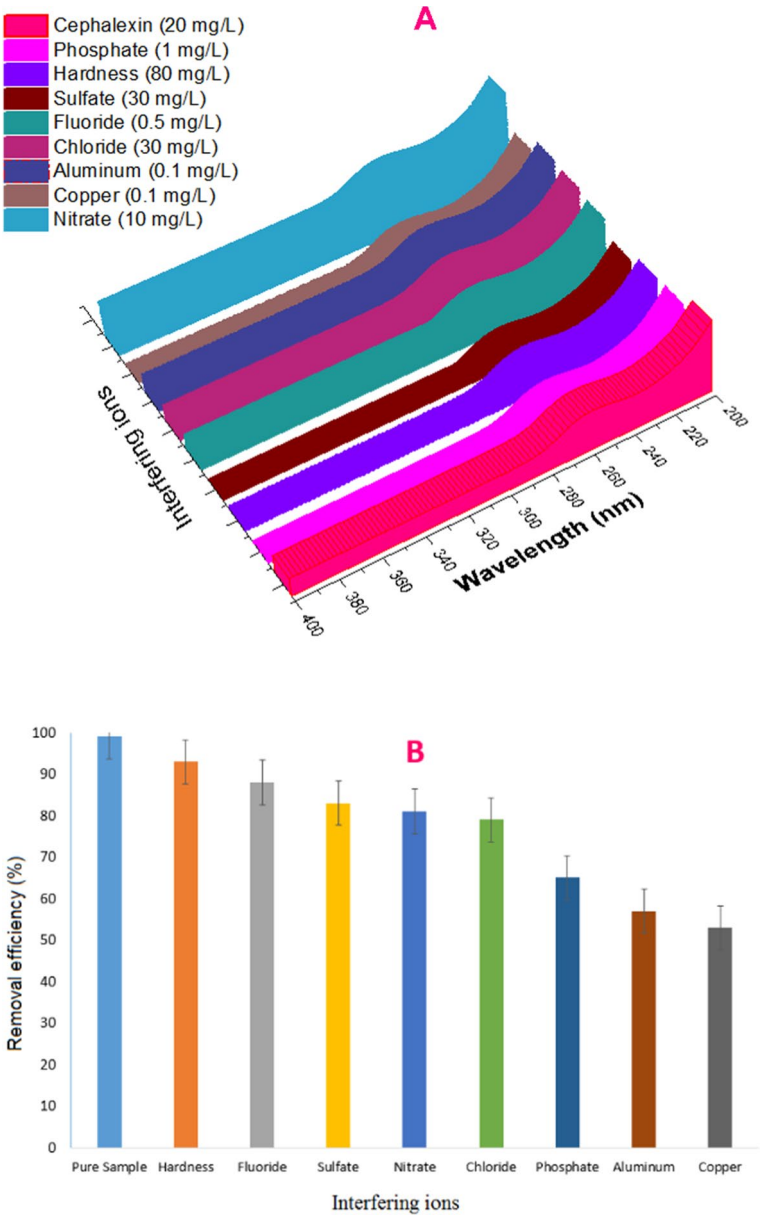

Fig. 8 UV/VIS of CEX after reacting with coexisting ions in the absence of adsorbent (**a**) and removal efficiency of CEX in the presence of adsorbent (**b**)

phenomenon may be due to the competing of anions and cations of salts with CEX ions to adsorb onto N-MCM-41 [44]. In addition, the formation of inner-sphere complex or outer-sphere complex may influence the ions sorption rate in the presence on foreign ions. The former is a complex in which ligands replace water molecules from the inner

coordination sphere and form bonds directly to solute ions. The latter is a complex in which there are no bonds between ligands and solute ions. For inner-sphere complex forming ions, increasing in ionic strength may increase the adsorption capacity or has no effect on adsorption capacity. On the other hand, outer-sphere complex forming ions leads to a decrease in the adsorption capacity for increasing ionic strength. The latter complex is formed mainly by electrostatic interactions and usually contains more than one water molecule between the solute and adsorbent functional groups [45]. Therefore, the decrease in CEX adsorption in the presence of interfering ions may be due to the formation of outer-sphere complex between CEX and N-MCM-41 adsorbent or competing effect of anions and cations of salts. The effect of salts on solution pH is another routes which influence the adsorption rate. The resulting salt solution may be neutral, but often it is acidic or basic. According to the Brønsted–Lowry concept of acids and bases, some ions can act as acids or bases. In this regard, sulfate, nitrate, chloride and phosphate was the anions of strong acid and thus will not affect the solution pH. These anions will reduce removal efficiency by competing with CEX to adsorb onto N-MCM-41. Removal of CEX decreased in the presence of highly charged metal cations such as aluminum, copper and hardness since they act as Brønsted–Lowry acid and therefore, decrease solution pH by producing hydronium ions in solution. Fluoride is anion of weak HF acid and therefore produce a basic solution. Therefore, the decreases in the removal efficiency of CEX in the presence of studied foreign anions may be due to the completing effect of anions, decrease on increase in solution pH and ionic strength [44].

Column adsorption study

In the present work, the nonlinear form of bed-depth-service-time (BDST) model which is known as the Thomas model (Eq. 1) was used to explain the dynamic adsorption of CEX onto N-MCM-41:

$$\frac{C_t}{C_o} = \frac{1}{1 + \exp\left[\left(\frac{k_{Th} q_e x}{Q}\right) - k_{Th} C_o t\right]} \tag{1}$$

where k_{Th} (mL/min mg) is the Thomas rate constant, q_e (mg/g) is the equilibrium solute uptake, C_o (mg/L) is the influent solute concentration, C_t (mg/L) is the effluent solute concentration at time t, x (g) is the mass of adsorbent and Q (mL/min) is the flow rate. The empty bed contact time (EBCT) and carbon usage rate (CUR) could be calculated from Eqs. 2 and 3 as follow:

$$\text{EBCT} = \frac{V_B}{Q} \tag{2}$$

$$\text{CUR} = \frac{M}{V} \tag{3}$$

where V_B is the volume of adsorbent (mL), Q(mL/min) is the flow rate, M is the adsorbent mass (g) and V is the volume of flow (mL). The effect of flow rate, column

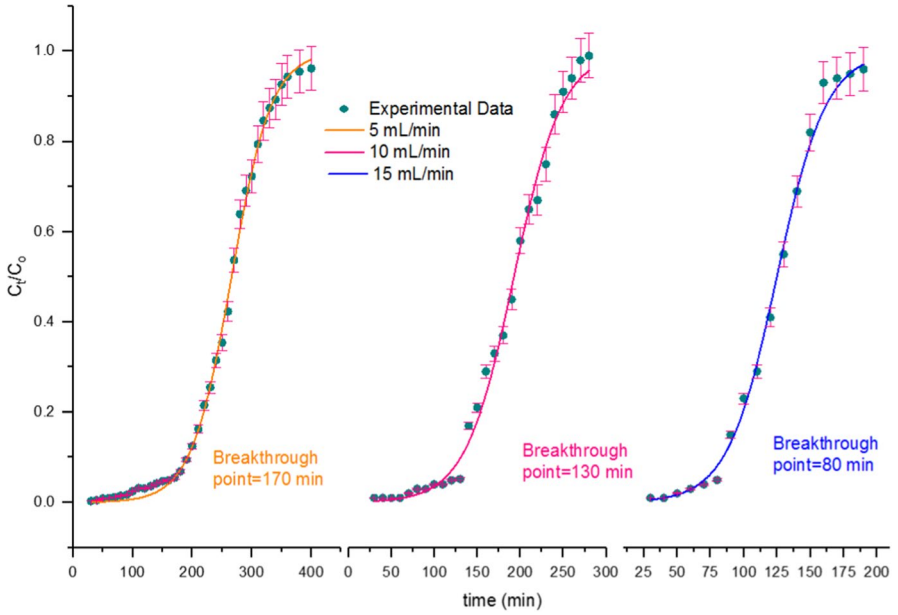

Fig. 9 Breakthrough curves expressed as C_t/C_o versus time for the sorption of CEX onto N-MCM-41 at different flow rates (initial concentration = 10 mg/L; bed height = 10 cm; adsorbent mass = 9.3 g)

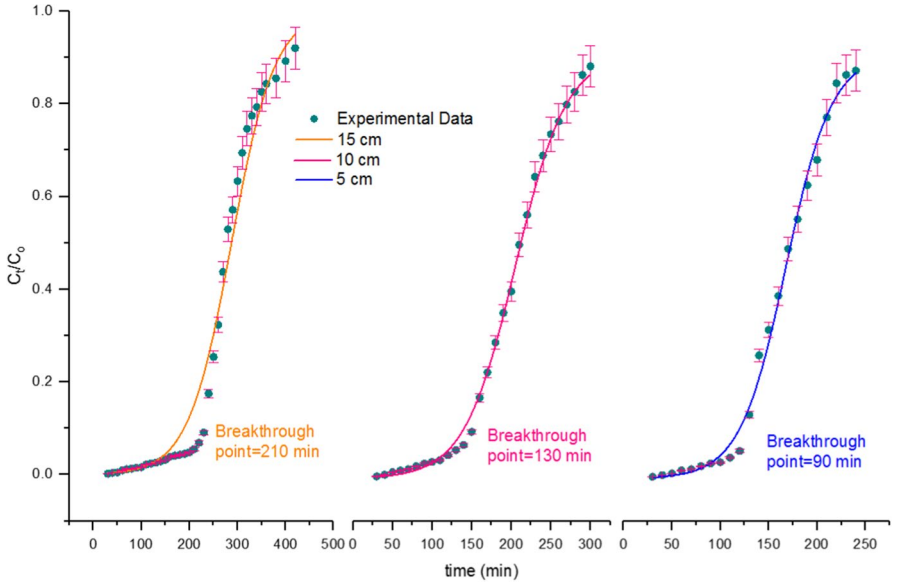

Fig. 10 Breakthrough curves expressed as C_t/C_o versus time for the sorption of CEX onto N-MCM-41 at different bed heights (initial concentration = 10 mg/L; flow rate = 10 mL/min)

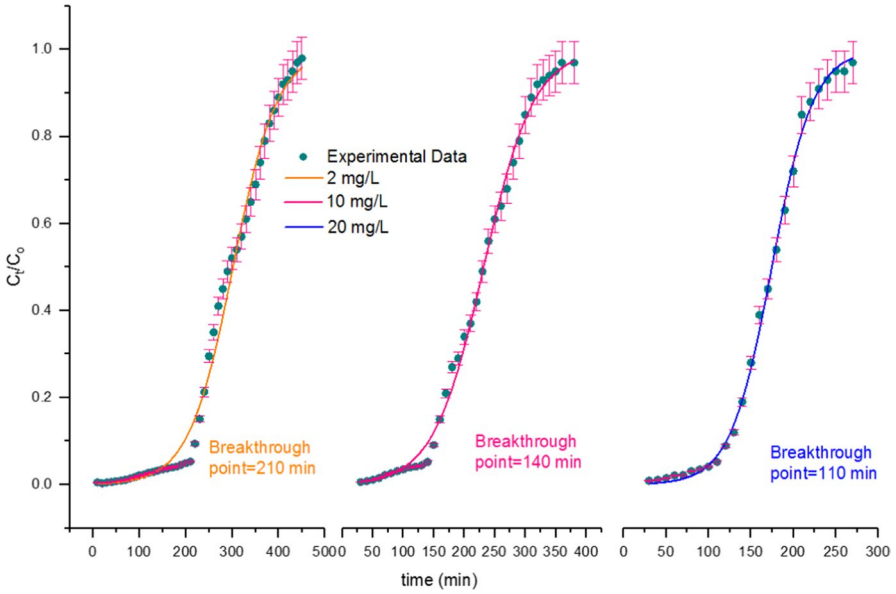

Fig. 11 Breakthrough curves expressed as C_t/C_o versus time for the sorption of CEX onto N-MCM-41 at different initial concentrations (bed height = 10 cm; flow rate = 10 mL/min)

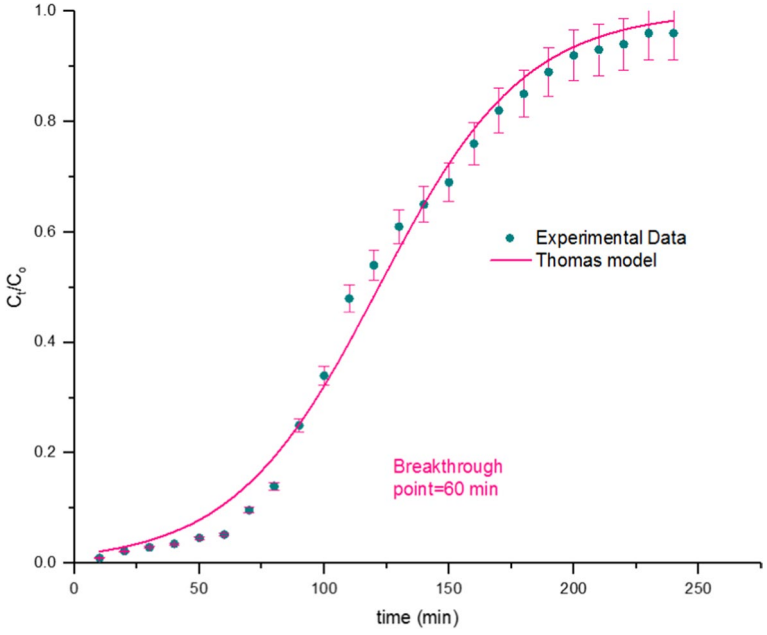

Fig. 12 Breakthrough curves expressed as C_t/C_o versus time for the sorption of CEX onto N-MCM-41 using the simulated sample (initial concentration = 10 mg/L; bed height = 10 cm; flow rate = 10 ml/min)

height, initial CEX concentration and competing ions on breakthrough curves are shown in Figs. 9, 10, 11 and 12. The parameters of nonlinear Thomas model are collected in Table 5. The breakthrough time was the time when $C_t/C_o = 0.05$ and the column exhaust time was the time $C_t/C_o = 0.90$. From Table 5, breakthrough curves fit well with Thomas model; demonstrating a good agreement of predicted breakthrough curves with experimental data for all studied parameters. The breakthrough point time was increased with decreasing flow rate (Fig. 9). With increasing flow rate from 5 to 15 mL/min the value of q_e decreased from 51.47 to 24.87 mg/g. This phenomenon can be attributed to the lower mass transfer time for adsorption of CEX onto binding sites at higher flow rate. Controversially, the rate constant (K_{Th}) of Thomas model was increased as flow rate increased; demonstrating lower mass transfer resistance at higher flow rate [46]. Another important factor that affect CEX adsorption is column heights which is directly proportional to the mass of adsorbent in the column [47]. The breakthrough point time increased from 90 min to 210 with increasing bed heights from 5 to 15 cm and corresponding rate constant (K_{Th}) values decreased (Fig. 10). Accordingly, adsorption capacity increased from 27.58 to 62.17 mg/g. The reason for higher adsorption capacity at elevated column heights is due to the more available adsorption sites for solute adsorption [33]. By varying the initial CEX concentration from 2 to 20 mg/L breakthrough point time occurred faster, while adsorption capacity increased from 24.52 to 57.43 mg/g (Fig. 11). This is due to the increase in driving force from solution to adsorption sites which resulted higher adsorption capacity at higher solute concentration [48]. Finally, to investigate the capability of prepared adsorbent in real condition, simulated sample ("Batch adsorption experiment" section) was passed from column (Fig. 12). In this regard, adsorption capacity was the lowest (19.74) and breakthrough point

Table 5 Parameters of Thomas model for CEX adsorption by N-MCM-41 in a fixed bed column

Parameters						
		K_{Th}(mL/mg min)	EBCT (min)	CUR (g/L)	q_e (mg/g)	R^2
$H = 10$ cm	5 mL/min	0.0024	1.57	4.65	51.47	0.99
C_o=10 mg/L	10 mL/min	0.0035	0.78	3.32	32.46	0.98
Adsorbent = 9.3 g	15 mL/min	0.0054	0.52	3.26	24.87	0.99
Flow = 10 ml/min	5 cm	0.0042	0.39	1.92	27.58	0.99
C_o= 10 mg/L	10 cm	0.0033	0.78	3.1	41.53	0.98
	15 cm	0.0022	1.18	4.45	62.17	0.98
Flow = 10 mL/min	2 mg/L	0.0053	0.785	2.06	24.52	0.99
$H = 10$ cm	10 mg/L	0.0037	0.785	2.44	32.34	0.99
Adsorbent = 9.3 g	20 mg/L	0.0031	0.785	3.44	57.43	0.99
Simulated Sample Flow = 10 ml/min $H = 10$ cm C_o= 10 mg/L Adsorbent = 9.3 g		0.00125	0.78	3.87	19.74	0.99

time occurred faster if compared with synthetic solution. The reason for the lowest adsorption capacity and breakthrough point time in simulated sample is due to the competing effect of foreign ions with CEX molecules to adsorb on adsorption sites and sample condition (pH and ionic strength) as explained in Sect. "Effect of coexisting ions."

Regeneration of N-MCM-41

To investigate the reusability of exhausted N-MCM-41, regeneration test was conducted on spent adsorbent from column study. Thermal destruction method was selected to regenerate the used adsorbent since CEX destruction rate increased linearly as temperature increased [48]. To do this, solution containing 10 mg/L CEX was passed from 10 cm column with flow rate of 10 ml/min. The exhausted N-MCM-41 from such column experiment was collected and refluxed at 110 °C in deionized water for 2 h. Finally, the recovered adsorbent was dried at 105 °C for 24 h and used in column mode to investigate the regeneration efficiency. The regeneration-reusability cycles were repeated until the adsorbent loosed 30% of initial capacity. Fig.S6 shows the regeneration cycle and loosed adsorption capacity of recovered adsorbent during six cycles. Adsorption capacity decreased from 41.53 to 8.72 mg/g at the end of six cycle regeneration. This is due to the detachment of amine functional group, filling of pores on the surface of adsorbent by small fraction of CEX fragments and adsorbent loses during regeneration experiment which ultimately resulted a reduction in adsorption capacity.

Conclusions

High specific surface area MCM-41 adsorbent was derived from Iranian natural pumice as an abundant, accessible, and inexpensive source of silica for the first time and highly grafted with APTES for anchoring cephalexin molecules. The parent MCM-41 had a specific surface of 913 m^2/g while the value decreased to 819 m^2/g after with grafting 6.52 µmol APTES per square meter of adsorbent surface. The XRD, FTIR, TGA and FESEM-EDX- Elemental mappings approved the amine group in the structure of adsorbent. According to Schiff base reaction, strong bonding of amine functionalization was achieved in the presence of TEOS as co-hydrolyzer and elevated temperature as accelerator of APTES hydrolyze. The N-MCM-41 showed excellent adsorption capacity for CEX in batch and dynamic condition. In this regard, 56.31 mg/g and 41.53 mg/g adsorption capacity was achieved in batch and dynamic condition, respectively. Removal efficiency was decreased by 50% in the presence of coexisting ions and simulated sample. Facile thermal destruction method demonstrated the regeneration of spent adsorbent for about six cycle. Overall, the present work could be used as an index for preparation of mesoporous silica-based adsorbent, grafting with amine group and used as antibiotics adsorbent.

Supplementary Information The online version contains supplementary material available at https://doi.org/10.1007/s00289-023-04685-w.

Acknowledgements This work was financially supported by Alborz University of Medical Sciences under 1394.01.05.1139.

Declarations

Conflict of interests The author declares that he has no known competing financial interests or personal relationships that could have appeared to influence the work reported in this paper.
The author declares that there are no conflicts of interest including any financial, personal, or other relationships with other people or organizations.

References

1. Lu D, Xu S, Qiu W, Sun Y, Liu X, Yang J, Ma J (2020) Adsorption and desorption behaviors of antibiotic ciprofloxacin on functionalized spherical MCM-41 for water treatment. J Clean Prod 264:121644
2. Rizzi V, Gubitosa J, Fini P, Nuzzo S, Cosma P (2020) Amino-grafted mesoporous MCM-41 and SBA-15 recyclable adsorbents: Desert-rose-petals-like SBA-15 type as the most efficient to remove azo textile dyes and their mixture from water. Sustain Mater Technol 26:e00231
3. Loganathan S, Tikmani M, Mishra A, Ghoshal AK (2016) Amine tethered pore-expanded MCM-41 for CO_2 capture: experimental, isotherm and kinetic modeling studies. Chem Eng J 303:89–99
4. Ebrahimi-Gatkash M, Younesi H, Shahbazi A, Heidari A (2017) Amino-functionalized mesoporous MCM-41 silica as an efficient adsorbent for water treatment: batch and fixed-bed column adsorption of the nitrate anion. Appl Water Sci 7:1887–1901
5. Mohseni-Bandpei A, Eslami A, Kazemian H, Zarrabi M, Javad Al-Musawi T (2020) A high density 3-aminopropyltriethoxysilane grafted pumice-derived silica aerogel as an efficient adsorbent for ibuprofen: Characterization and optimization of the adsorption data using response surface methodology. Environ Technol Innov 18:100642
6. Yıldız MG, Davran-Candan T, Günay ME, Yıldırım R (2019) CO_2 capture over amine-functionalized MCM-41 and SBA-15: exploratory analysis and decision tree classification of past data. J CO2 Util 31:27–42
7. Nazari G, Abolghasemi H, Esmaieli M (2016) Batch adsorption of cephalexin antibiotic from aqueous solution by walnut shell-based activated carbon. J Taiwan Inst Chem Eng 58:357–365
8. Shirani Z, Song H, Bhatnagara A (2020) efficient removal of diclofenac and cephalexin from aqueous solution using Anthriscus sylvestris-derived activated biochar. Sci Total Environ 745:140789
9. Samarghandi MR, Javad Al-Musawi T, Mohseni-Bandpi A, Zarrabi M (2015) Adsorption of cephalexin from aqueous solution using natural zeolite and zeolite coated with manganese oxide nanoparticles. J Mol Liq 21:431–441
10. Rabanimehr F, Farhadian M, Solaimany Nazar AR (2022) a high-performance microreactor integrated with chitosan/ Bi2WO6/CNT/TiO2 nanofibers for adsorptive/photocatalytic removal of cephalexin from aqueous solution. Int J Biol Macromol 208:260–274
11. Tavasol F, Tabatabaie T, Ramavandi B, Amiri F (2021) Photocatalyst production from wasted sediment and quality improvement with titanium dioxide to remove cephalexin in the presence of hydrogen peroxide and ultrasonic waves: a cost-effective technique. Chemosphere 284:131337
12. Leili M, Shirmohammadi Khorram N, Godini K, Azarian G, Moussavi R, Peykhoshian A (2020) Application of central composite design (CCD) for optimization of cephalexin antibiotic removal using electro-oxidation process. J Mol Liq 313:113556
13. Wang B, Li H, Liu T, Guo J (2021) Enhanced removal of cephalexin and sulfadiazine in nitrifying membrane-aerated biofilm reactors. Chemosphere 263:128224
14. Sierra RSC, Zúñiga-Benítez H, Peñuela GA (2021) Elimination of cephalexin and doxycycline under low frequency ultrasound. Ultrason Sonochem 79:105777
15. Wang KY, Xiao Y, Chung TS (2006) chemically modified polybenzimidazole nanofiltration membrane for the separation of electrolytes and cephalexin. Chem Eng Sci 61:5807–5817
16. Mahreni M, Ramadhan RR, Pramadhana MF, Permatasari AP, Kurniawati D, Kusuma HS (2022) Synthesis of metal organic framework (MOF) based Ca-Alginate for adsorption of malachite green dye. Polym Bull 79:11301–11315

17. Neolaka YAB, Supriyanto G, Kusuma HS (2018) Adsorption performance of Cr(VI)-imprinted poly(4-VP-co-MMA) supported on activated Indonesia (Ende-Flores) natural zeolite structure for Cr(VI) removal from aqueous solution. J Environ Chem Eng 6:3436–3443
18. Vrancken KC, Possemiers K, Voort PVD, Vansant EF (1995) Surface modification of silica gels with aminoorganosilanes. Colloids Surf A 98:235–241
19. Noori Sepehr M, Zarrabi M, Kazemian H, Abdeltif A, Yaghmaian K, Ghaffari HR (2013) Removal of hardness agents, calcium and magnesium, by natural and alkaline modified pumice stones in single and binary systems. Appl Surf Sci 274:295–305
20. Thommes M, Kaneko K, Neimark AV, Olivier JP, Rodriguez-Reinoso F, Rouquerol J, Sing KSW (2015) Physisorption of gases, with special reference to the evaluation of surface area and pore size distribution (IUPAC technical report). Pure Appl Chem 87:1051–1069
21. Shariatinia Z, Pourzadi N, Darvishi SMR (2021) tert-Butylamine functionalized MCM-41 mesoporous nanoparticles as drug carriers for the controlled release of cyclophosphamide anticancer drug. Surf Interfaces 22:100842
22. Mohseni-Bandpei A, Eslami A, Kazemian H, Zarrabi M, Venkataraman S, Sadani M (2022) Enhanced adsorption and recyclability of surface modified hydrophobic silica aerogel with triethoxysilane: removal of cefixime by batch and column mode techniques. Environ Sci Pollut Res. https://doi.org/10.1007/s11356-022-22277-5
23. Liu Y, Li C, Peyravi A, Sun Z, Zhang G, Rahmani K, Zheng S, Hashisho Z (2021) Mesoporous MCM-41 derived from natural Opoka and its application for organic vapors removal. J Hazard Mater 408:124911
24. Bao Y, Yan X, Du W, Xie X, Pan Z, Zhou J, Li L (2015) Application of amine-functionalized MCM-41 modified ultrafiltration membrane to remove chromium (VI) and copper (II). Chem Eng J 281:460–467
25. Goscianska J, Olejnik A, Nowak I (2017) APTES-functionalized mesoporous silica as a vehicle for antipyrine—adsorption and release studies. Colloids Surf A: Physicochem Eng Asp 533:187–196
26. Akshay SM, Samanta AN (2019) Amine-impregnated MCM-41 in post-combustion CO_2 capture: synthesis, characterization, isotherm modelling. Adv Powder Technol 30:3231–3240
27. Mashhadizadeh MH, Amoli-Diva M (2012) Drug-carrying amino silane coated magnetic nanoparticles as potential vehicles for delivery of antibiotics. J Nanomed Nanotechnol 3:2–7
28. Aissaoui N, Bergaoui L, Landoulsi J, Lambert JF, Boujday S (2012) Silane layers on silicon surfaces: mechanism of interaction, stability, and influence on protein adsorption. Langmuir 28:656–665
29. Araghi SH, Entezari MH (2015) Amino-functionalized silica magnetite nanoparticles for the simultaneous removal of pollutants from aqueous solution. Appl Surf Sci 333:68–77
30. Rezaei B, Havakeshian E, Ensafi AA (2013) Stainless steel modified with an aminosilane layer and gold nanoparticles as a novel disposable substrate for impedimetric immunosensors. Biosens Bioelectron 48:61–66
31. Alsalbokh M, Fakeri N, Lawson S, Rownaghi AA, Rezaei F (2021) Adsorption of iodine from aqueous solutions by aminosilane-grafted mesoporous alumina. Chem Eng J 415:128968
32. Pasternack RM, Amy SR, Chabal YJ (2008) Attachment of 3-(Aminopropyl)triethoxysilane on silicon oxide surfaces: dependence on solution temperature. Langmuir 24:12963–12971
33. Cuoq F, Masion A, Labille J, Rose J, Ziarelli F, Prelot B, Bottero JY (2013) Preparation of amino-functionalized silica in aqueous conditions. Appl Surf Sci 266:155–160
34. Zhu M, Lerum MZ, Chen W (2012) How to prepare reproducible, homogeneous, and hydrolytically stable aminosilane-derived layers on silica. Langmuir 28:416–423
35. Mohseni-Bandpi A, Javad Al-Musawi T, Ghahramani E, Zarrabi M, Mohebi S, Abdollahi Vahed S (2016) Improvement of zeolite adsorption capacity for cephalexin by coating with magnetic Fe_3O_4 nanoparticles. J Mol Liq 218:615–624
36. Saremi F, Miroliaei MR, Shahabi Nejad M, Sheibani H (2020) Adsorption of tetracycline antibiotic from aqueous solutions onto vitamin B6-upgraded biochar derived from date palm leaves. J Mol Liq 318:114126
37. Bouhedda M, Lefnaoui S, Rebouh S, Yahoum MM (2019) Predictive model based on Adaptive Neuro-Fuzzy Inference System for estimation of Cephalexin adsorption on the Octenyl Succinic Anhydride starch, Chemom. Intell Lab Syst. https://doi.org/10.1016/j.chemolab.2019.103843
38. Zhao Y, Zhao H, Zhao X, Qub Y, Liu D (2020) Synergistic effect of electrostatic and coordination interactions for adsorption removal of cephalexin from water using a zirconium-based metal-organic framework. J Colloid Interface Sci 580:256–263

39. Zarrabi M, Soori MM, Noori Sepehr M, Amrane A, Borji S, Ghaffari HR (2014) Removal of phosphorus by ion-exchange resins: equilibrium, kinetic and thermodynamic studies. Environ Eng Manag J 13:205–214
40. Neolaka YAB, Lawa Y, Naat J, Riwu AAP, Darmokoesoemo H, Widyaningrum BA, Iqbal M, SeptyaKusuma H (2021) Indonesian Kesambi wood (*Schleichera oleosa*) activated with pyrolysis and HSO combination methods to produce mesoporous activated carbon for Pb(II) adsorption from aqueous solution. Environ Technol Innov 24:101997
41. Al-Khalisy RS, Al-Haidary AMA, Al-Dujaili AH (2010) Aqueous phase adsorption of cephalexin onto bentonite and activated carbon. Sep Sci Technol 45:1286–1294
42. Miao MS, Liu Q, Shu L, Wang Z, Liu YZ, Kong Q (2016) Removal of cephalexin from effluent by activated carbon prepared from alligator weed: kinetics, isotherms, and thermodynamic analyses, Process Saf. Environ 104:481–489
43. Hashemzadeh F, Ariannezhad M, Derakhshandeh SH (2022) Evaluation of Cephalexin and Amoxicillin removal from aqueous media using activated carbon produced from *Aloe vera* leaf waste. Chem Phys Lett 800:139656
44. Aranda-García E, Chávez-Camarillo GM, Cristiani-Urbina E (2020) Effect of ionic strength and coexisting ions on the biosorption of divalent nickel by the Acorn Shell of the Oak *Quercus crassipes* Humb. & Bonpl. Processes 8:1229–1246
45. Karimaian KA, Amrane A, Kazemian H, Panahi R, Zarrabi M (2013) Retention of phosphorous ions on natural and engineered waste pumice: characterization, equilibrium, competing ions, regeneration, kinetic, equilibrium and thermodynamic study. Appl Surf Sci 284:419–431
46. Amiri MJ, Khozaei M, Gil A (2019) Modification of the Thomas model for predicting unsymmetrical breakthrough curves using an adaptive neural-based fuzzy inference system. J Water Health 17:25–36
47. Nazari G, Abolghasemi H, Esmaieli M, Sadeghi Pouya E (2016) aqueous phase adsorption of cephalexin by walnut shell-based activated carbon: a fixed-bed column study. App Surf Sci 375:144–153
48. Ayub A, Ahsan S, Meeroff D, Jahandar Lashaki M (2022) Amine-grafted mesoporous silica materials for single-stage biogas upgrading to biomethane. Chem Eng J 445:136497